Plasma Enhanced Terahertz Rectification and Noise in InGaAs HEMTs

Javier Mateos, *Member, IEEE*, and Toms González, *Senior Member, IEEE*

***Abstract*—In this work, we explore high frequency collective phenomena present in InGaAs HEMTs which lead to a peak in the current noise spectrum and enhance their DC response to THz signals, thus originating a resonance in the rectification of AC signals. These phenomena have been evidenced in recent experiments, in which THz detection as a result of plasma wave resonances has been demonstrated. In this paper, by means of Monte Carlo simulations, the noise spectra and the AC–DC rectification properties of the devices have been calculated and linked to the properties of the plasma oscillations within two distinct parts of the source-gate region: the capped and the recessed sections of the channel.**

***Index Terms*—InGaAs high electron mobility transistors (HEMTs), Monte Carlo simulation, plasma oscillations, THz detection.**

I. Introduction

THE range of the electromagnetic spectrum, sandwiched between microwaves and infrared light, with frequencies between 300 GHz and 3 THz (sometimes called T-rays), has gained scientific and commercial interest in recent years due to its broad range of potential applications, which were previously restricted to radioastronomy and high resolution spectroscopy [1]. The fast development of new technologies, such as pump–probe time-domain THz spectroscopy with ultra-fast lasers [2] or ultra-high frequency MMICs based on aggressively scaled InGaAs HEMTs and HBTs [3], [4], is making practically available THz systems working at room temperature. The applications which are presently being focused are mainly security-screening tools [5], [6], but also ultra high speed communications and medical imaging (without the damage produced by ionizing radiation such as X-rays). THz sources must be obtained at the limits of electronics from one side and optical systems from the other, resulting in a lack of efficient and practical radiation sources, which most of the times need bulky (or low temperature) equipment. In the last years, the search for more powerful alternatives to the frequency multiplication of electronic sources or the photomixing of optical beams has come to the possibility of exploiting the use of plasma resonances in semiconductor devices in order to fabricate compact room temperature THz sources and detectors. This approach has been confirmed by recent experiments made with classic high electron mobility transistors (HEMTs) based on different material systems (GaAs, InGaAs and GaN), and Si MOSFETs, where THz detection as a result of plasma wave resonances has been demonstrated [7], [8]. Also, some evidence of plasma related THz emission has been found [9], [10].

Up to now, only ideally simple 1D theoretical models, not considering the complex geometry and electron dynamics in HEMTs, have been used for predicting the different types of plasma resonances that can appear in semiconductor devices [7], [11]–[13]. In this work, we try to explain the mechanism of plasma-resonant THz detection with HEMTs by means of 2D Monte Carlo (MC) simulations self-consistently coupled with a Poisson solver [14]–[16]. This technique is able to consider the real geometry and layer structure of the HEMTs and provide not only static results but also identify the effect of collective phenomena such as plasma oscillations on both the current noise and the AC–DC rectification properties of the devices. The in-house MC simulator has been already validated through comparison with experimental results obtained in similar devices and concerning static characteristics, small-signal and noise parameters [10], [14].

In previous works [17], [18], MC simulations of an extremely simple device, the so called self-switching diode (SSD), have confirmed the presence of a peak in the current noise spectral density with a dependence on the geometry similar to that exhibited by an analogous peak observed in the AC–DC rectification. These are two different evidences of the same internal phenomena: plasma resonances. In this work, we will show, by means of MC simulations, how this very same relationship between AC–DC rectification and noise linked to plasma oscillations holds also in classical InGaAs based HEMTs, where the phenomena are even more complex due to the presence of a third electrode. In both cases, SSDs and HEMTs, the plasma-related charge fluctuations in regions where the field effects limit the current flowing through the devices establish a link between the noise in the current (given by the plasma oscillations) and the AC–DC rectification (given by the coupling between the internal plasma and the external DC output signal). This work summarizes and completes the theoretical interpretation of the preliminary results presented by the authors in two prior conference papers [15], [16].

II. MC Model and Devices Under Study

The most appropriate numerical technique to deal with room temperature nanometer-size devices where electron transport is potentially ballistic is the MC method, able to provide static results and also the dynamic and noise behavior of the structures. Thus, to model the devices we make use of a 2D MC, consisting

Manuscript received March 15, 2012; revised July 16, 2012; accepted July 16, 2012. Date of publication August 23, 2012; date of current version August 30, 2012. This work has been supported in part by European Comission through the ROOTHz Project ICT-2009-243845, by the Direccion General de Investigacion (MICINN) through Project TEC2010-15413, and by the Cosejeria de Educacion, Junta de Castilla y Leon through Project SA183A12-1.

The authors are with the Departamento de Física Aplicada, Universidad de Salamanca, 37008 Salamanca, Spain (e-mail: javierm@usal.es).

Color versions of one or more of the figures in this paper are available online at http://ieeexplore.ieee.org.

Digital Object Identifier 10.1109/TTHZ.2012.2209970

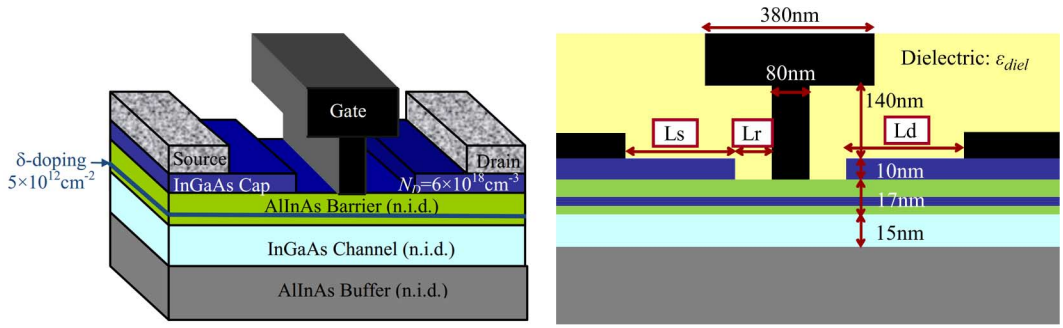

Fig. 1. (a) Layer structure and geometry of the simulated HEMTs based on InGaAs channels. (b) 2D simulation domain and main dimensions.

of a semiclassical ensemble MC simulator self-consistently coupled with a 2D Poisson solver. The MC transport description is based on a 3-valley model (Γ-L-X nonparabolic spherical valleys for both InGaAs and AlInAs) and includes ionized impurity, alloy, polar and non-polar optical phonon, acoustic phonon and intervalley scattering, and appropriate carrier injection techniques at the contacts. Details about the model can be found in [14].

The geometry of the simulated 80 nm T-gate InGaAs HEMTs is shown in Fig. 1 and is based on that already used in [10]. This recessed topology is similar to that commonly used in fabricated devices. The length of the source, recess and drain regions (Ls, Lr and Ld, respectively) will be taken as variable parameters in the MC simulations to understand their influence on the plasma effects. Surface charges at the semiconductor-air interfaces, σ, are included in a simple way by fixing the value of σ to the experimentally-extracted equilibrium value, keeping it constant independently of the topology of the structure, bias and time [14]. Simulations are performed at $T = 300$ K.

In order to model the THz detection mechanism (AC–DC conversion), as in [12], a sinusoidal signal of varying frequency is superimposed to the DC gate bias, $V_{\rm gs}$, and the average drain current is recorded. The detection of the AC signal is therefore accounted for as an increment of the drain current, ΔI_d. On the other hand, noise calculations are carried out in the standard way. First, from the time series of instantaneous current values obtained from the simulation we evaluate the autocorrelation function of current fluctuations. Then, by Fourier transform, the corresponding spectral density is calculated. To this end, the dynamics of electrons in the device have been simulated during time series of 500.000 steps of 1 fs for each bias point.

III. Physics of Plasma-Resonant THz Detection

Initially the results for the AC–DC response will be presented. Fig. 2 shows the variation of the drain current with respect to its static value, ΔI_d, as a function of the frequency of a sinusoidal signal (of amplitude 0.1 V) superimposed to different DC values of $V_{\rm gs}$ in a HEMT with $Ls = 200$ nm, $Lr = 100$ nm and $Ld = 0.5$ μm (the different curves have been shifted by 20 A/m each to enhance the clarity of the figure). As observed ΔI_d shows a resonant peak (mainly for $V_{\rm gs}$ near pinch off) for a frequency around 2.5 THz, in good agreement with similar experimental measurements [19], [20]. In Sections V and Section VI, the origin and frequency of this peak will be

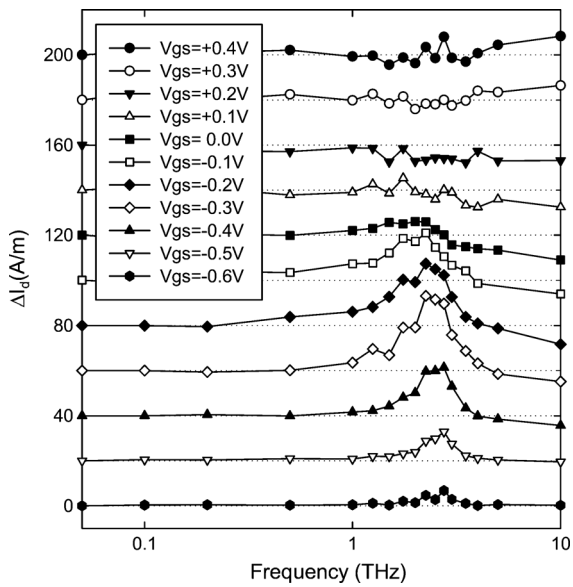

Fig. 2. Average drain–current variation originated by the superposition of a sinusoidal signal of 0.1 V of amplitude and varying frequency to the DC gate potential ($V_{\rm gs}$) of a HEMT with $Ls = 200$ nm, $Lr = 100$ nm and $Ld = 0.5$ μm. The different curves have been shifted by 20 A/m each. $V_{ds} = 1.0$ V.

explained in terms of different plasma modes that are possible in the HEMT.

In order to perform the comparison between the noise of a device and its response to oscillating signals, it must be bear in mind that the spectral density of current fluctuations at equilibrium is related to its small signal behavior [21], whereas the DC response current is caused by the device rectification and corresponds to large signal (nonlinear) operating conditions. As such, the amplitude of the signal superimposed to the DC gate voltage has been kept to a low value of 0.1 V (but high enough to produce a significant response for ΔI_d).

The resonance between the plasma oscillations in the source-gate region of the HEMT and the excitation applied to the gate voltage is clearly visible in the time evolution of the potential and carrier concentration profiles obtained with the MC simulations, shown in Fig. 3. Fig. 3(a) and 3(b) show that at low frequency the potential and electron concentration under the gate are in phase (a lower gate potential induces a lower electron concentration). But at the frequency of the resonance, Fig. 3(c) and 3(d), due to the plasma oscillations within the source–gate region, the injection of the electrons under the gate is in opposite

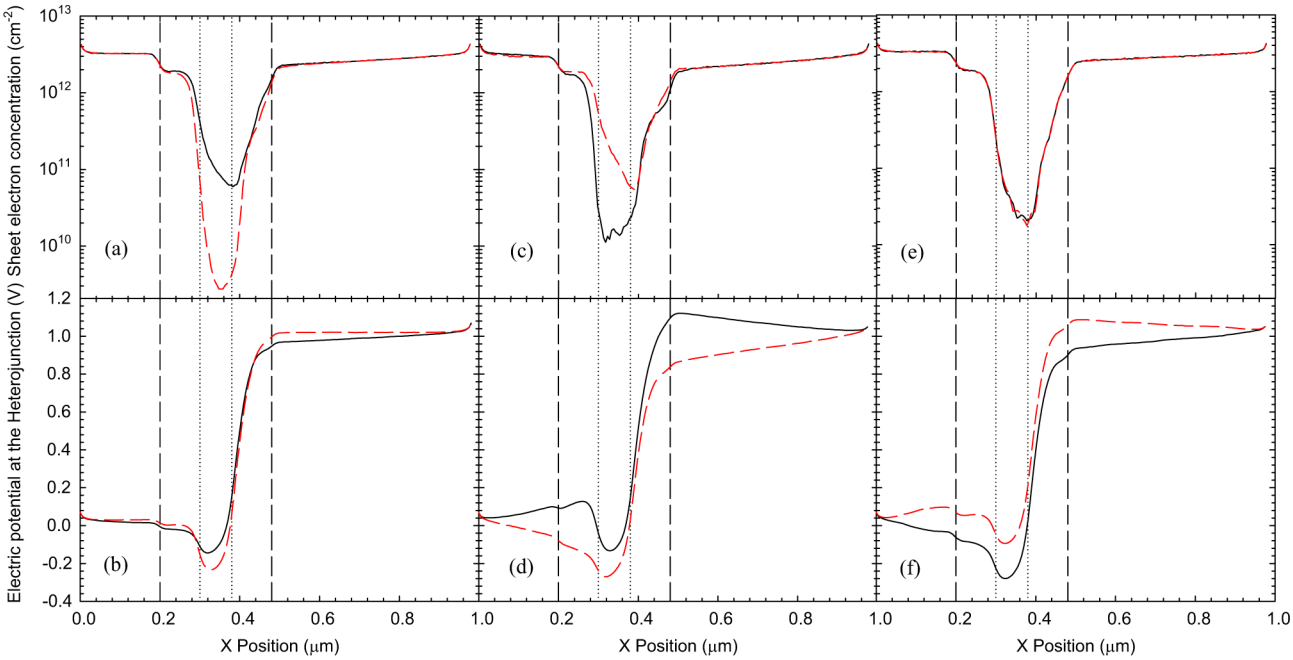

Fig. 3. Instantaneous profiles of (a), (c), and (e) sheet electron concentration in the channel and (b), (d), and (f) electric potential at the heterojunction of a HEMT with $Ls = 200$ nm, $Lr = 100$ nm and $Ld = 0.5$ μm when sinusoidal AC signals (amplitude 0.1 V) are superimposed to the DC gate bias ($V_{\rm gs} = -0.3$ V) with frequencies of: (a), (b) 1.0 THz; (c), (d) 2.5 THz (corresponding to the resonant peak); and (e), (f) 10.0 THz. Dashed-red/solid-black lines correspond to the time moment when the applied gate voltage is maximum/minimum within a period. The position of the gate and recess are shown by vertical dotted and dashed lines, respectively, and the insets show a magnification of the electron concentration within the source region of the HEMT. The time-domain evolution of the profiles is available in the web as supplemental material. $V_{ds} = 1.0$ V.

phase to the gate potential variations. As a consequence, when the gate potential decreases the electron concentration is higher, thus increasing the drain current over its stationary value. This effect is mainly visible at gate voltages near pinch off, since it is the nonlinearity of the transfer curve which provides a net positive variation of drain current when such an "opposite phase" evolution of potential and electron concentration arises. Finally, at very high frequencies the electron concentration does not respond to the changes in the potential profile, Fig. 3(e) and 3(f), thus leading to a zero value of ΔI_d.

IV. Link Between Noise and Rectification

For having a deeper insight into the origin of the plasma-resonant detection we have performed simulations of HEMTs with different geometries for $V_{\rm gs} = -0.3$ V, the value of gate bias that provides the optimum AC–DC response. Fig. 4(a) shows the results for the HEMT previously analyzed in Fig. 2 compared with those obtained for devices with a longer gate of 0.2 μm and a longer drain region of 1 μm. It can be observed that the frequency of the resonant peak does not depend on the gate length, Lg, nor on the recess-drain region, Ld. On the contrary, the resonant frequency strongly depends on the lengths of the recess-source region, Ls, Fig. 4(b), and of the source side of the recess, Lr, Fig. 4(c). Moreover, the resonant frequency variation with Lr is stronger than with Ls; it increases from 1.5 to more than 3 THz when reducing the value of Lr from 300 to 10 nm. These results clearly indicate that the source-gate region (including the recess) acts as the plasma-wave cavity that produces the resonant detection of THz radiation in HEMTs. This fact is confirmed by the comparison of the frequency dependence of the source, gate and drain current noise spectra, S_{Is}, S_{Ig} and S_{Id}, respectively, with that of $\Delta I_d(f)$ shown in Fig. 5 for a HEMT with $Lr = 100$ nm and $Ld = 0.5$ μm and different values of Ls. Fig. 5 evidences the presence of a peak in all the three S_{Is}, S_{Ig} and S_{Id}, analogous to that observed in the case of the rectifying response. However, the dependence of the frequency of the peak in the noise spectra with the length of the source region Ls is analogous to that observed for $\Delta I_d(f)$ only for the case of S_{Is}, and not for S_{Ig} and S_{Id}. This happens because it is the resonance between the plasma-related charge fluctuations of the source-gate region and the oscillating gate voltage that results in ΔI_d, due to an enhanced injection of electrons over the potential barrier induced by the gate electrode. In fact, the very same characteristic frequency is also visible in the spectra of the electric potential fluctuations in the channel under the source side of the gate (not shown here), which is the point that determines the value of I_d, since it is where the carrier injection over the potential barrier takes place.

As can be expected, the peak of S_{Id} observed in Fig. 5(c) is related to the electron dynamics within the drain region and its position depends on its length Ld (results not shown here) in the same way as S_{Is} depends on Ls. However, as explained above, such plasma oscillations in the drain region do not couple to $\Delta I_d(f)$ as the source ones do.

It is also remarkable the degradation of the quality factor of the resonant peak observed in Fig. 4(b) as the length of the source region is increased (the FWHM, Full Width at Half Maximum, of the peaks increases), which goes in parallel to the broadening of the peak of the source current noise. This is also observed when the recess region is enlarged, Fig. 4(c), and it is due to the more efficient damping of the plasma resonance by scattering as the size of the resonant cavity increases.

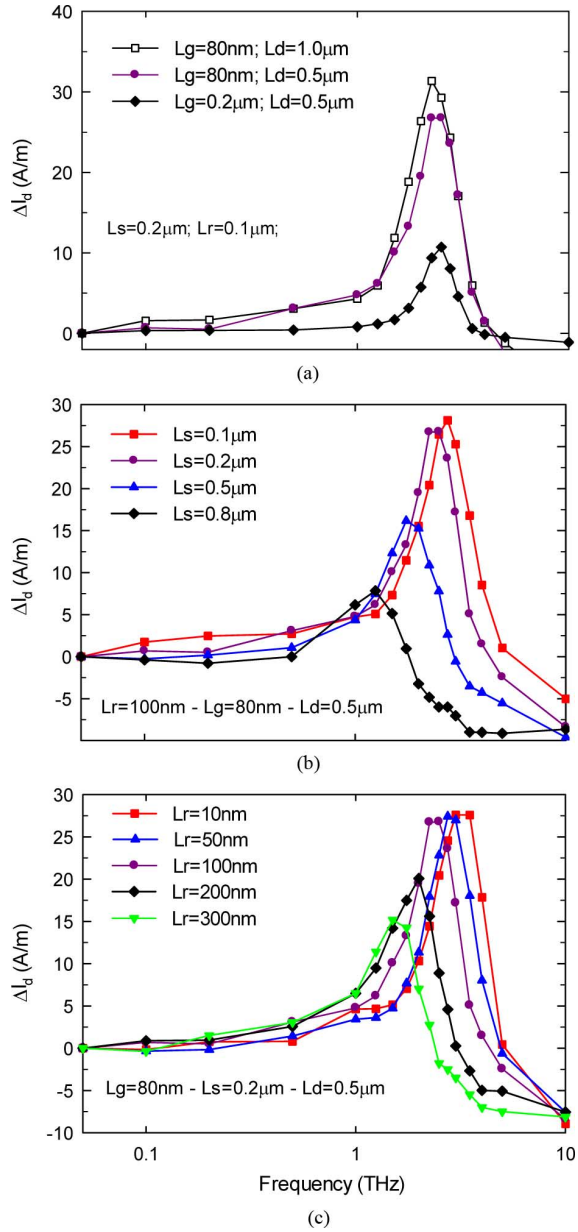

Fig. 4. ΔI_d vs. frequency for $V_{gs} = -0.3$ V and $V_{ds} = 1.0$ V for HEMTs with different (a) Ld and Lg, (b) Ls and (c) Lr.

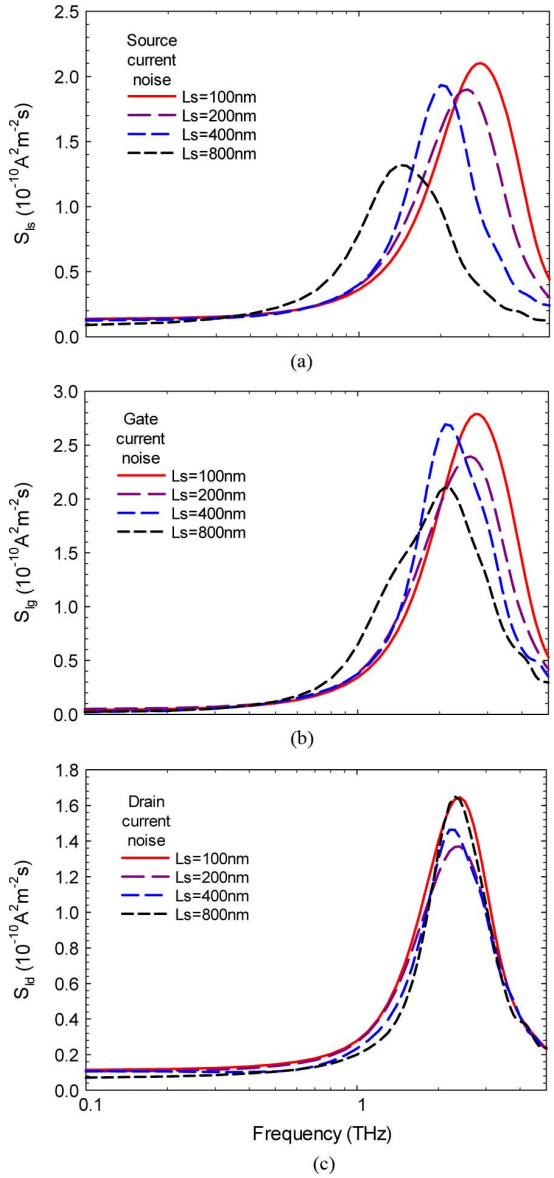

Fig. 5. Comparison between: (a) source; (b) gate; and (c) drain–current noise spectra, S_{Is}, S_{Ig}, and S_{Id}, respectively, and the frequency dependent drain–current AC–DC conversion, in a HEMT with $Lr = 100$ nm and $Ld = 0.5$ μm and different values of Ls ($V_{gs} = -0.3$ V, $V_{ds} = 1.0$ V).

A further confirmation is provided by the results of Fig. 6, which shows the bias dependence of the frequency of the resonant peak of $\Delta I_d(f)$ compared with those of the peaks observed in the source, gate and drain current noise spectra for different values of Ls. As observed, the frequency of the resonant peak in both $\Delta I_d(f)$ and S_{Is} shifts towards lower values as V_{gs} is increased (as already seen in Fig. 2). The variation with Ls is also coincident, thus confirming the close relationship between source current noise and AC–DC rectification. On the contrary, the peak frequency of S_{Id} does not depend on the source-gate distance, since it is mainly affected by the drain region of the device. The behavior of the peak in S_{Ig} also somewhat follows that of the plasma resonant rectification, but not as closely as that of S_{Is}, mainly for the longest values of Ls Fig. 6(c).

For an ideally long source region, the plasma resonance (and the peak in S_{Is}) should practically not depend on the gate voltage, since V_{gs} does not in principle affect the electron concentration in that region. This is observed in Fig. 6(c), in which $Ls = 400$ nm and the resonant frequency hardly changes with V_{gs}. However, when the source length is shortened, the lateral depletion induced by the gate voltage can significantly modify the size of the plasma cavity, thus appreciably modulating the resonant frequency. A higher gate potential reduces the depletion, so that the effective length $Ls + Lr$ is increased and the plasma frequency decreases. This effect is more evident for the shortest source regions, Fig. 6(b) for $Ls = 200$ nm and mainly Fig. 6(a) for $Ls = 100$ nm.

V. 2D Plasma Frequencies in HEMTs

Dyakonov–Shur theory predicts the values of the plasma frequencies that should appear when mobile charges with effective mass $m*$ are distributed in an ideally thin channel

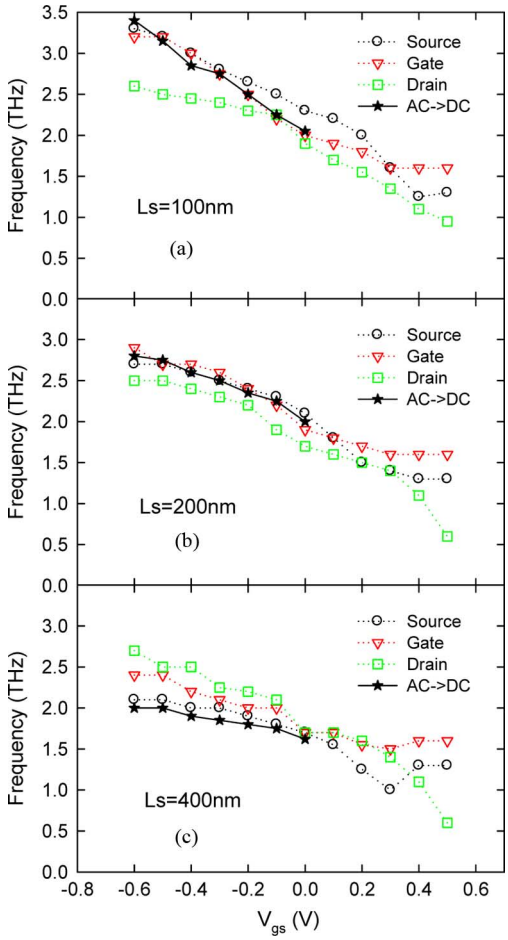

Fig. 6. Gate bias dependence of the frequency of the resonant AC–DC conversion peak compared with those of the source, gate and drain current noise spectrum maximums for HEMTs with $Lr = 100$ nm and $Ld = 0.5$ μm and (a) $Ls = 100$ nm, (b) $Ls = 200$ nm and (c) $Ls = 400$ nm. $V_{ds} = 1.0$ V.

sandwiched by a dielectric material with permittivity ε_{diel} (2D case), and when a gate contact is placed at a distance d from the channel (gated 2D case); see, for example, [22]. Their values are, respectively

$$\text{2D plasma}: \quad f_p = \frac{1}{2\pi}\sqrt{\frac{e^2 n_{2D} k}{2m^* \varepsilon_{diel}\varepsilon_0}} \tag{1}$$

$$\text{Gated 2D plasma}: \quad f_p = \frac{1}{2\pi}\sqrt{\frac{e^2 n_{2D} d}{m^* \varepsilon_{diel}\varepsilon_0}k} \tag{2}$$

where k being the plasma wave vector, ε_0 the vacuum permittivity and n_{2D} the sheet electron density. The mechanisms at the origin of plasma oscillations in a sheet of electrons are analogous to those of waves in fluids, since both can be represented by hydrodynamic equations. Indeed, these cases of 2D and gated 2D plasma oscillations can be understood as analogous to deep water and shallow water waves, respectively.

Due to the complex geometry of the simulated HEMT and the different plasma modes that may appear in the source-gate region, sketched in Fig. 7, there is not a unique ideal plasma model for explaining the MC results (mainly because the source–gate region is made up by the series combination of the source and recess regions, with lengths Ls and Lr, respectively).

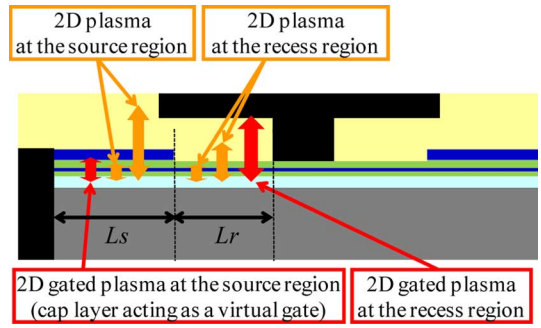

Fig. 7. Representation of the different possible 2D plasma modes in the source–gate region of the recessed T-gate HEMT. Ungated 2D plasma modes are shown in orange while the gated ones are shown in red. The source and recess regions are also indicated.

Moreover, there are two possible ungated plasma modes (both on the source and the recess regions): on the one hand one can consider that electromagnetic coupling takes place through the semiconductor forming the barrier itself (AlInAs, with $\varepsilon_{\text{diel}} = 13.88$), on the other hand there is also the possibility that it takes place at a longer scale and therefore one has to consider the external dielectric (in this case SiN, typically used for the passivation of HEMTs, with $\varepsilon_{diel} = 6$). Also, in addition to the gated plasma mode that could come out within the recess region due to the presence of the gate hat (with $d = 167$ nm), as suggested in [7], the highly-doped source cap region acts as a quasi-metallic constant voltage region, thus possibly generating a 2D gated plasma in that part of the device (with $d = 17$ nm). In Fig. 8 the theoretical dependences of the different plasma modes [see (1) and (2)] are plotted using the following criteria:

- The value of $k = \pi/2L$, with $L = Ls + Lr$, has been used because: 1) as explained before, the plasma-wave cavity corresponds to the source-gate region and 2) as shown in Fig. 3, the boundary conditions for the electric potential variations is a fixed value at the left and oscillating potential at the right (nearly open circuit, since the channel is almost pinched off). Therefore the source-gate region corresponds to a $\lambda/4$ distance and as such k takes the value $\pi/2(Ls + Lr)$.
- The values of n_{2D} in the channel are different in the source region and under the recess. We have used here the values obtained from the MC simulations (see Fig. 3), of 3.1×10^{12} and 1.8×10^{12} cm^{-2}, respectively.
- For the gated 2D plasma at the recess region we have used $d = 167$ nm (channel-gate hat distance) while at the source $d = 17$ nm (channel-cap distance).

The comparison between the ideal dependences with those obtained from MC simulations shown in Fig. 8 allows extracting interesting information. The dependence of the resonant frequency when varying Ls is similar to the $1/\sqrt{L}$ behavior of the 2D plasma case, while when varying Lr, the dependence approaches the $1/L$ trend characteristic of the gated 2D plasma. These dependences seem to be in agreement with the geometry of the HEMT, since the recess is covered by the gate contact while the source region is not. However, this contradicts the fact that nearly the same dependencies on Ls and Lr are obtained with MC simulations performed without considering the T-shape of the gate electrode (shown in Fig. 8 by open symbols),

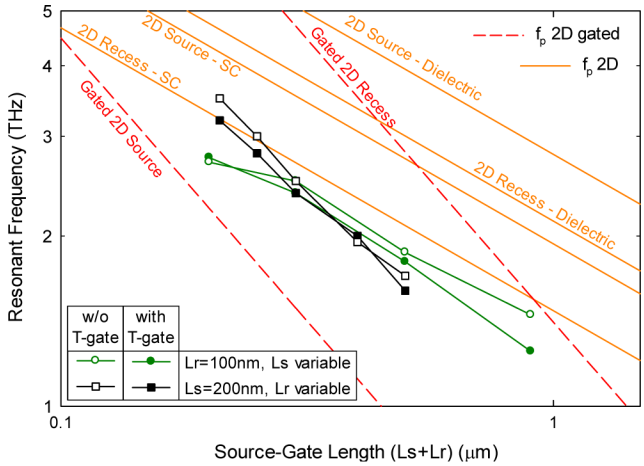

Fig. 8. Frequencies of the different possible plasma modes in the source and recess regions of the HEMT versus source-gate length as compared with the MC results of the resonant peak in the AC–DC conversion. The results of MC simulations without considering the T shape of the gate are also shown by open symbols. For the ungated 2D plasma modes (both at the recess and source regions) the coupling via both the semiconductor (SC) forming the barrier ($\varepsilon_{\rm diel} = 13.88$) and the dielectric outside the HEMT ($\varepsilon_{\rm diel} = 6$) are plotted. $Lg = 80$ nm and $Ld = 500$ nm.

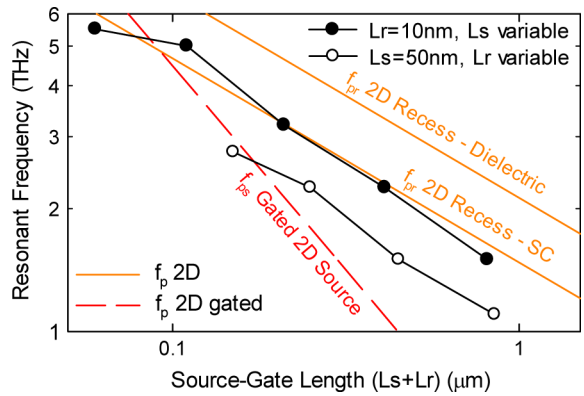

Fig. 9. Values of the plasma frequencies in the source and recess regions of the HEMT vs. source-gate length as compared with the MC results of the resonant peak in the AC–DC conversion for $Lr = 10$ nm and variable Ls (so that $Ls \gg Lr$) and $Ls = 50$ nm and variable Lr (so that $Ls \ll Lr$).

where the possibility of the 2D-gated mode in the recess region is cancelled. Moreover, the 2D-gated mode within the source region, caused by the cap acting as a virtual gate, seems to be necessary to explain the MC results (in good agreement with the results of the hydrodynamic model presented in [7]), since it is the only one providing plasma frequencies below the values obtained from the MC simulations. Therefore, the combination of this mode with that of the recess region is the more plausible possibility to originate the resonances shown in the MC simulations. Regarding the recess region, both coupling possibilities (via the AlInAs barrier and the external dielectric) are considered, even if the latter one provides excessively high values of the ungated 2D plasma mode. The exact way the plasma frequencies of the source and recess regions combine themselves to generate the overall plasma-resonant detection in HEMTs will be explored in the next section.

VI. Series Combination of Plasma Modes

The previous MC results indicate that the origin of the resonant AC–DC conversion is a series combination of plasma modes in the source and recess regions: 1) a gated 2D plasma mode in the source region as a result of the coupling between the channel and the cap layer and 2) a 2D plasma mode within the recess region.

The case of a series connection of two regions with different plasma frequencies has already been studied in the simple case of n^+nn^+ diodes, where the 3D plasma frequency of the n^+ regions is different from that of the n-region [23]. In that case the overall peak observed in the current fluctuations appears at an intermediate frequency lying between the 3D plasma values of the two regions considered independently. A phenomenological analytical formula able to predict the global plasma frequency, $f_{2\rm reg}$, as a function of the length of each of the two regions has been suggested [24]. We will apply that formula to our case in this way

$$f_{2reg}^2 = f_{ps}^2 \frac{Lr}{Ls+Lr} + f_{pr}^2 \frac{Ls}{Ls+Lr} \tag{3}$$

where f_{ps} and f_{pr} being the plasma frequencies corresponding to the source and recess regions, respectively.

Equation (3) predicts that if $Ls \gg Lr$ then $f_p \longrightarrow f_{pr}$ and if $Ls \ll Lr$ then $f_p \longrightarrow f_{ps}$. In order to check this behavior we have performed simulations of those extreme cases: 1) with $Lr = 10$ nm and variable Ls and 2) $Ls = 50$ nm and variable Lr. In Fig. 9 we compare these results with the ideal 2D plasma mode in the source region and the two possible 2D plasma modes within the recess region (following the previous discussion the ungated 2D mode in the source region and the gated 2D in the recess have been disregarded). In the case when $Ls \ll Lr$, the MC results are close to f_{ps}, but do not follow the expected gated 2D dependence. This discrepancy is attributed to the fact that being $Ls = 50$ nm, such short cap is not able to completely fix the potential, so that the "virtual gate" is not effective. In the case when $Ls \gg Lr$ the results are very close to f_{pr} considering the ungated 2D coupling short recess region, $Lr = 10$ nm). From this last result one could expect that the dielectric outside the semiconductor has no effect on the plasma resonant detection. In order to verify its influence, we have performed MC simulations with different dielectric materials placed at the top of the device. The typical SiN dielectric used for the passivation of the HEMTs with $\varepsilon_{diel} = 6.0$ (which has been considered in all the previous cases) has been changed by $\varepsilon_{\rm diel} = 1.0$ and 13.88, corresponding, respectively, to air and InGaAs. The results of these simulations, Fig. 10, show that the value of the resonant frequency increases when decreasing the permittivity of the dielectric placed on the top of the active layers of the HEMT, as expected from (1).

Fig. 10 also shows the comparison of the MC results with those of (3) in which f_{ps} and f_{pr} have been obtained through the analytical formulas given in (2) and (1), corresponding to gated and ungated 2D plasma modes, respectively, following the previous considerations. For simplicity, in the case of the ungated plasma mode, the value of $\varepsilon_{\rm diel} = 13.88$ has been used, so that

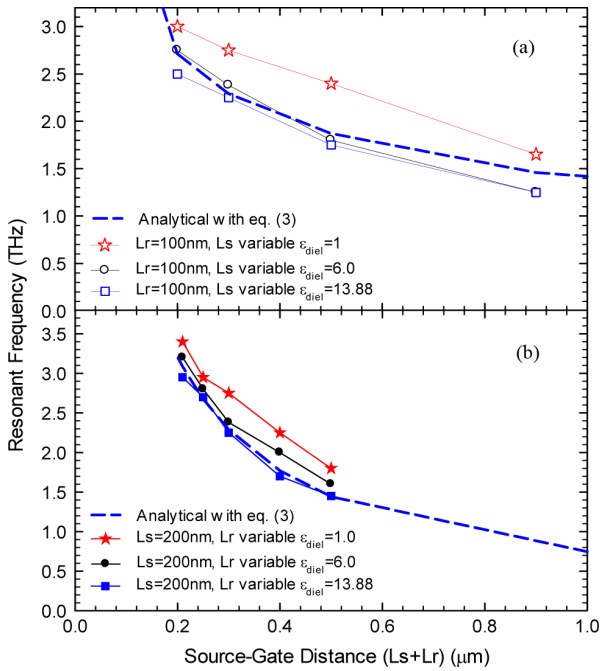

Fig. 10. Resonant frequency of the AC–DC conversion in HEMTs as a function of the source-gate distance with (a) varying Ls and constant $Lr = 100$ nm and (b) varying Lr and constant $Ls = 200$ nm, obtained with MC simulations using three different dielectrics at the top of the device. $Lg = 80$ nm and $Ld = 500$ nm. The analytical dependence obtained with (3) and $\varepsilon_{\rm diel} = 13.88$ is also plotted by dashed lines.

the comparison should be made with that MC case. In order to reach the observed good agreement, the limit between the two regions has been slightly shifted towards the source side (20 nm), which can be understood as a border effect of the "virtual gate". These results confirm that: i) the plasma mode appearing in the recess region is not only the result of the coupling between the channel and the semiconducting barrier (as seems to happen for the shortest recess lengths, Fig. 9) since the dielectric outside the devices plays also a significant role (mainly for long Lr) and ii) for sufficiently long values of Ls, the efficiency of the cap layer acting as a "virtual gate" increases, thus exciting the gated 2D plasma mode in that region.

The results presented in this paper indicate that the plasma resonance in the source-gate region of HEMTs enhances their responsivity for the detection of THz signals, which can therefore be adequately tuned in frequency by choosing the topology of the source and recess regions. This clearly demonstrates the possibility of practically applying such transistors for the selective detection of THz waves.

VII. Conclusion

By means of MC simulations we have described the mechanism for the plasma-resonant THz detection observed in HEMTs and linked it to the noise in the source current. Simulations show that the peak of the current noise spectra and the resonant frequency of the AC–DC conversion depend similarly on the topology of the devices and are a consequence of plasma oscillations of free charge in the source-gate region of the HEMT. This peak in the THz detection observed in HEMTs is a result of a combination of the plasma modes of two distinct regions, the source region, with the cap layer acting as a "virtual gate" (thus leading to 2D-gated plasma oscillations) and the recess region, where an ungated 2D plasma mode arises. The combination of the two modes has been explained through a phenomenological formula, previously derived for n^+nn^+ diodes.

References

[1] , D. Mittleman, Ed., *Sensing With THz Radiation*. New York: Springer-Verlag, 2003.
[2] E. R. Brown, F. W. Smith, and K. A. McIntosh, "Coherent millimeter-wave generation by heterodyne conversion in low-temperature-grown GaAs photoconductors," *J. Appl. Phys.*, vol. 73, p. 1480, 1993.
[3] L. A. Samoska, "An overview of solid-state integrated circuit amplifiers in the submillimeter-wave and THz regime," *IEEE Trans. THz Sci. Technol.*, vol. 1, no. 1, pp. 9–24, Sep. 2011.
[4] W. R. Deal, X. B. Mei, K. Leong, V. Radisic, S. Sarkozy, and R. Lai, "THz monolithic integrated circuits using InP high electron mobility transistors," *IEEE Trans. THz Sci. Technol.*, vol. 1, no. 1, pp. 25–32, Sep. 2011.
[5] , R. E. Miles, X. -C. Zhang, H. Eisele, and A. Krotkus, Eds., *Terahertz Frequency Detection and Identification of Materials and Objects*. New York: Springer, 2007.
[6] R. Appleby and H. B. Wallace, "Standoff detection of weapons and contraband in the 100 GHz to 1 THz region," *IEEE Trans. Antennas Propag.*, vol. 55, no. 11, pt. 1, pp. 2944–2956, Nov. 2007.
[7] P. Nouvel, H. Marinchio, J. Torres, C. Palermo, D. Gasquet, L. Chusseau, L. Varani, P. Shiktorov, E. Starikov, and V. Gruzhinskis, "Terahertz spectroscopy of plasma waves in high electron mobility transistors," *J. App. Phys.*, vol. 106, p. 013717, 2009.
[8] W. Knap, M. Dyakonov, D. Coquillat, F. Teppe, N. Dyakonova, J. Lusakowski, K. Karpierz, M. Sakowicz, G. Valusis, D. Seliuta, I. Kasalynas, A. El Fatimy, Y. M. Meziani, and T. Otsuji, "Field Effect Transistors for terahertz detection: Physics and first imaging application," *J. Infrared Millim. THz Waves*, vol. 30, pp. 1319–1337, 2009.
[9] S. Boubanga-Tombet, F. Teppe, J. Torres, A. El Moutaouakil, D. Coquillat, N. Dyakonova, C. Consejo, P. Arcade, P. Nouvel, H. Marinchio, T. Laurent, C. Palermo, A. Penarier, T. Otsuji, L. Varani, and W. Knap, "Room temperature coherent and voltage tunable terahertz emission from nanometer-sized field effect transistors," *Appl. Phys. Lett.*, vol. 97, p. 262108, 2010.
[10] J. Lusakowski, W. Knap, N. Dyakonova, L. Varani, J. Mateos, T. Gonzalez, Y. Roelens, S. Bollaert, A. Cappy, and K. Karpierz, "Voltage tuneable terahertz emission from a ballistic nanometer InGaAs/InALAs transistor," *J. Appl. Phys.*, vol. 97, p. 064307, 2005.
[11] M. Dyakonov and M. S. Shur, "Shallow water analogy for a ballistic field effect transistor: New mechanism of plasma wave generation by dc current," *Phys. Rev. Lett.*, vol. 71, pp. 2465–2468, 1993.
[12] M. Dyakonov and M. S. Shur, "Detection, mixing, and frequency multiplication of terahertz radiation by two dimensional electronic fluid," *IEEE Trans. Electron Devices*, vol. 43, no. 3, pp. 380–387, Mar. 1996.
[13] V. Ryzhii, A. Satou, W. Knap, and M. S. Shur, "Plasma oscillations in high-electron-mobility transistors with recessed gate," *J. Appl. Phys.*, vol. 99, p. 084507, 2006.
[14] J. Mateos, D. Pardo, T. González, V. Hoel, and A. Cappy, "Monte Carlo simulator for the design optimization of low-noise HEMTs," *IEEE Trans. Electron. Devices*, vol. 47, no. 10, pp. 1950–1956, Oct. 2000.
[15] J. Mateos, H. Marinchio, C. Palermo, L. Varani, and T. González, "Plasma-resonant THz detection with HEMTs," in *Proc. 2010 22nd Int. Conf. on Indium Phosphide and Related Mater. (IPRM)*, May 2010, pp. 1–4.
[16] J. Mateos, I. Iñiguez-de-la-Torre, and T. González, "Noise and terahertz rectification in semiconductor diodes and transistors," in *Proc. IEEE 21st Int. Conf. on Noise and Fluctuations (ICNF 2011)*, Jun. 2011, pp. 16–21.
[17] I. Iñiguez-de-la-Torre, J. Mateos, D. Pardo, A. M. Song, and T. González, "Noise and terahertz rectification linked by geometry in planar asymmetric nanodiodes," *Appl. Phys. Lett.*, vol. 94, p. 093512, 2009.
[18] I. Iñiguez-de-la-Torre, J. Mateos, D. Pardo, and T. González, "Monte Carlo analysis of noise spectra in self-switching nanodiodes," *J. Appl. Phys.*, vol. 103, p. 024502, 2008.

[19] A. El Fatimy, F. Teppe, N. Dyakonova, W. Knap, D. Seliuta, G. Valušis, A. Shchepetov, Y. Roelens, S. Bollaert, A. Cappy, and S. Rumyantsev, "Resonant and voltage-tunable THz detection in InGaAs/InP nanometer transistors," *Appl. Phys. Lett.*, vol. 89, p. 131926, 2006.

[20] A. El Fatimy, J. C. Delagnes, A. Younus, E. Nguema, F. Teppe, W. Knap, E. Abraham, and P. Mounaix, "Plasma wave field effect transistors as a resonant detector for imaging applications up to one terahertz for 1 terahertz imaging applications," *Opt. Commun.*, vol. 282, pp. 3055–3058, 2009.

[21] D. Gasquet, M. De Murcia, J. P. Nougier, and C. Gontrand, "Transport parameters of hot electrons in GaAs at 300 K," *Phys. B*, vol. 134, pp. 264–268, 1985.

[22] M. S. Shur and V. Ryzhii, "Plasma wave electronics," in *Terahertz Sensing Technology. Volume 1: Electronic Devices and Advanced Systems Technology*, D. L. Woolard, W. R. Loerop, and M. S. Shur, Eds. , Singapore: World Scientific, 2003, ch. 7.

[23] P. Ziadé, H. Marinchio, T. Laurent, G. Sabatini, Z. Kallassy, C. Palermo, and L. Varani, "Hydrodynamic study of terahertz three-dimensional plasma resonances in InGaAs diodes," *Semicond. Sci. Technol*, vol. 25, p. 075012, 2010.

[24] L. Reggiani, P. Golinelli, E. Faucher, L. Varani, T. González, and D. Pardo, V. Bareikis and R. Katilius, Eds., "Plasma and transit-time effects on electronic noise in semiconductor n^+nn^+ structures," in *Proc. 13th Int. Conf. of Noise in Physical Syst. and 1/f Fluctuations*, Singapore, 1995, p. 193.

Javier Mateos (M'09) was born in Salamanca, Spain, in 1970. He received the B.S. and Ph.D. degrees in physics from the University of Salamanca, Salamanca, Spain, in 1993 and 1997, respectively.

Since 1993, he has been with the Department of Applied Physics, University of Salamanca, Spain, becoming an Associate Professor in 2000. He is presently Coordinator of the EU project ROOTHz aiming at fabricating THz emitters and detectors using semiconductor nanodevices. His current research interests also include the development of novel device concepts using ballistic transport and HEMTs based in both narrow and wide bandgap III–V semiconductors. He is the author or coauthor of more than 90 refereed scientific journal papers and 140 conference contributions.

Tomás González (M'05–SM'07) was born in Salamanca, Spain, in 1967. He received the B.S. and Ph.D. degrees in physics from the University of Salamanca, Salamanca, Spain, in 1990 and 1994, respectively.

Since 1991, he has been with the Department of Applied Physics at the University of Salamanca, where he is currently a Full Professor of Electronics. He is the author or coauthor of more than 125 refereed scientific journal papers and 170 conference presentations. His research interests include high-frequency III-V transistors, microscopic modeling of electronic noise, and development of novel THz device concepts based on ballistic transport.

Dr. Gonzáles serves on the committees of several international conferences (ICNF, EDISON).